3

The role of radar in predicting and preventing asteroid and comet collisions with Earth

Steven J. Ostro
Jet Propulsion Laboratory, California Institute of Technology
Jon D. Giorgini
Jet Propulsion Laboratory, California Institute of Technology

1 Introduction

The current Spaceguard Survey classifies each known near-Earth asteroid (NEA) as either non-threatening or deserving of additional astrometric attention. For any possibly threatening object, the dominant issues are the uncertainty in its trajectory and physical nature as well as what can be done to reduce that uncertainty. Morrison *et al*. (2002) note that

> From the standpoint of an allocator of society's resources, an uncertain threat calls for adaptive policies, delaying potentially costly action but informing later decision by investing in uncertainty-reduction measures. In the context of the NEO impact hazard, this means avoiding the costs of standing organizational structures and capital expenditures until a threat materializes. . . .

Thus reduction in uncertainty is tantamount to ensuring that unnecessary costs are avoided and that necessary actions are undertaken with adequate warning.

Ground-based radar is a knowledge-gathering tool that is uniquely able to shrink uncertainty in NEO trajectories and physical properties. The power of radar stems largely from the precision of its measurements (Table 3.1). The resolution of echoes in time delay (range) and Doppler frequency (radial velocity) is often of order $1/100$ the extent of a kilometer-sized target, so several thousand radar image pixels can be placed on the target. Delay-Doppler positional measurements often have a fractional precision finer than $1/10\,000\,000$, comparable to sub-milliarcsecond optical astrometry.

The single-date signal-to-noise ratio (SNR) of echoes, a measure of the number of useful imaging pixels placed on a target by a given radar data set, depends primarily on the object's distance and size. Figure 3.1 shows nominal values of

Mitigation of Hazardous Comets and Asteroids, ed. M. J. S. Belton, T. H. Morgan, N. H. Samarasinha, and D. K. Yeomans. Published by Cambridge University Press.

Table 3.1 *Fractional precision of NEA radar measurements*[a]

	Range (m)	Radial velocity ($m\,s^{-1}$)
Best radar resolution	∼10	∼0.000 1
Echo dispersion	∼1 000	0.01 to 10
Astrometric "location"	∼10 000 000	∼10 000

[a] The optimal resolution of radar measurements of the distribution of echo power in time delay (range) and Doppler frequency (radial velocity) for observations of a large NEA is compared with the scale of the object's delay-Doppler extent and location.

SNR for Arecibo and Goldstone. Notwithstanding the heroic efforts by Zaitsev and colleagues in Russia and several intercontinental asteroid radar demonstrations involving Goldstone or Arecibo transmissions with reception of asteroid echoes in Japan, Spain, and Italy, the world's only effective NEO radars are at Arecibo and Goldstone, whose declination windows are -1° to 38° and $> -40^\circ$, respectively. However, given the historical funding difficulties experienced by those two systems (Beatty 2002), the future of radar astronomy cannot be taken for granted. Time will tell whether the USA will opt to maintain, much less improve, the current Arecibo and Goldstone radar telescopes.

In this chapter, we examine how our current radar capabilities might help at each stage of detecting and mitigating an impact hazard encountered during this century. See Ostro (1994) for a discussion of radar's role in hazard mitigation written a decade ago, Ostro *et al*. (2002) for a review of asteroid radar astronomy, and Harmon *et al*. (1999) for a review of comet radar astronomy.

2 Post-discovery astrometric follow-up

Once an asteroid is discovered, its orbital motion must be followed well enough to permit reliable prediction and recovery at the next favorable apparition. As of April 2004, 41% of the 595 identified Potentially Hazardous Asteroids (PHAs) are lost in the sense that the three-standard-deviation uncertainty in the time of the next close-approach exceeds ± 10 days, corresponding roughly to a plane-of-sky angular uncertainty greater than 90°. (A PHA is defined by NASA's Jet Propulsion Laboratory as an object having a minimum orbit intersection distance with the Earth ≤ 0.05 AU and an absolute visual magnitude $H \leq 22$.)

The first asteroid radar astrometry was obtained in 1968 (for 1566 Icarus) (Goldstein 1968; Pettengill *et al*. 1969). Prior to those observations, from simulations designed to evaluate the usefulness of optical and radar astrometry of Icarus in disclosing relativistic effects, Shapiro *et al*. (1968) concluded that radar data would

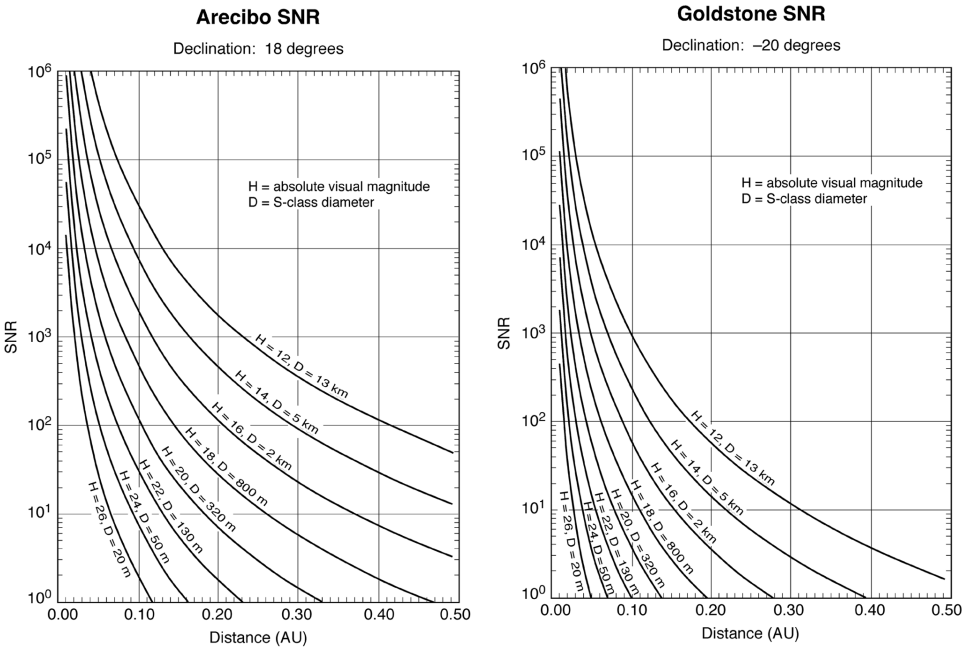

Figure 3.1 Predictions of the single-date signal-to-noise ratio (SNR): (a) for Arecibo echoes from asteroids at declination 18°, and (b) for Goldstone echoes from asteroids at declination −20°, as a function of the target's distance and absolute visual magnitude (converted to diameter by assuming an S-class optical albedo of 0.16) (Zellner 1979). Other assumptions include a 10% radar albedo, an equatorial view, a 4-h rotation period, and optimal values for system parameters. Plots for other declinations and distances are on the Internet (Ostro 2004a).

make an impressive contribution to the improvement of estimates of that asteroid's orbit. Two decades later, the potential of delay-Doppler measurements for small-body orbit refinement was examined comprehensively in a series of Monte Carlo simulations carried out by Yeomans *et al*. (1987). They showed that a single radar detection of a newly discovered NEA shrinks the instantaneous positional uncertainty at the object's next close approach by orders of magnitude with respect to an optical-only orbit, thereby preventing "loss" of the object. These conclusions have been substantiated quantitatively in the years since through comparison of radar+optical with optical-only positional predictions for recoveries of NEAs during the past decade (Table 3.2): The radar-based predictions historically have had pointing errors that average 310 times smaller than their optical-only counterparts, dramatically facilitating recovery.

Furthermore, radar astrometry can significantly reduce ephemeris uncertainties even for an object whose optical astrometry spans many decades. For example, radar measurements of 1862 Apollo (Ostro *et al*. 1991) at Arecibo showed that the object's optical-astrometry-based orbit, although based on 49 years of data, had

Table 3.2 *Residuals for past NEA recoveries*[a]

Object	Recovery date	O	R	O/R
1989 PB (4769 Castalia)	May 1990	24″	0.4″	60
1991 AQ	Sep 1994	57″	0.1″	380
1986 DA (6178)	Oct 1994	56″	0.9″	60
1991 JX (6489 Golevka)	Mar 1995	3600″	4.6″	780
1989 JA (7335)	Oct 1996	196″	99.3″	2
1986 JK (14827 Hypnos)	Apr 2000	114″	0.1″	910
1998 ML14	Nov 2002	125″	0.5″	250
1990 OS	Jun 2003	50477″	3200″	16

[a] Here O represents the positional offset (the observed position at recovery minus the predicted position) for a pre-recovery orbit solution incorporating only optical astrometry. R represents the residual for a pre-recovery orbit solution using radar combined with optical. O/R is the ratio of residuals for the two cases and is a measure of the relative reduction in position error when radar astrometry is included in the orbit solution.

a range error of 3750 $\pm$ 2 km. (See also the discussion of 1950 DA below.) The reduced uncertainties of a radar orbit can also aid recovery at fainter magnitudes. For example, 1998 ML14 was recovered (Table 3.2) at magnitude 21.2, only 0.5 arcseconds from the position predicted from a radar+optical orbit. The optical-only orbit would have suggested a search for the faint object 125 arcseconds away from the actual position.

For NEAs observed only during their discovery apparition, one can predict the uncertainty in the location during the next opportunity for optical observation, and hence the area of the sky for a search having a given likelihood of success. Table 3.3 lists the total sky area for the three-standard-deviation orbit-determination uncertainties mapped onto the sky at the next favorable Earth-based recovery date (which we define as the next time when the apparent visual magnitude is less than 20 during reasonable sky-brightness conditions) for both an optical-only orbit and a radar+optical orbit, for seven NEAs. Radar shrinks the required sky search area by an average factor of 2642, dramatically facilitating recovery. For six other objects in the table, the optical-only and radar+optical orbits are so different that the nominal recovery dates are months or years apart. Since the radar+optical solutions would be expected to be the more accurate, reliance on an optical-only solution would be unlikely to lead to recovery.

3 Window of predictability

A goal of the Spaceguard Survey is to provide as much warning as possible of any possibly dangerous approach of NEAs as large as 1 kilometer. However, since

Table 3.3 *Search areas for future NEA recoveries*

Object[a]	Most favorable Earth-based recovery date	Optical orbit recovery	Data span (days)	Astrometry			Gap (yrs)	Search area (arcsec^2)		
				Optical	Doppler	delay		O	R	O/R
1996 JG	Nov 26 2003	∼	20	265	3	3	7	1.5E5	310	484
2000 EH26	Jun 24 2005	∼	140	47	4	2	5	47808	1055	45
2002 FD6	Sep 23 2006	∼	15	556	2	4	4	3.9E5	146	2671
2002 BM26	Dec 20 2006	(2003)	87	218	2	2	4	–	294	–
2000 UG11	Oct 24 2008	(2025)	19	395	1	2	8	–	70	–
2001 AV43	Oct 21 2013	∼	182	46	1	0	12	1.5E5	6.1E4	2
2002 FC	Jul 08 2021	∼	137	191	3	1	19	14297	35	408
1998 KY26	May 31 2024	∼	11	211	2	2	26	33534	786	43
2000 RD53	Oct 15 2031	∼	102	322	5	4	31	89005	6	14834
2002 AV	Jan 25 2033	(2036)	39	210	3	2	31	–	816	–
2000 LF3	May 31 2046	(2090)	13	67	4	1	46	–	1.1E5	–
1999 TY2	Oct 03 2064	(2091)	5	115	1	0	65	–	2.3E6	–
2001 FR85	Mar 09 2081	(2082)	7	36	3	1	80	–	9.5E4	–

[a] The objects listed above were observed optically and with radar over a single apparition. We used least-squares to estimate optical-only and radar+optical orbits and then used the radar+optical orbit to determine a likely recovery date, defined as the next time when the apparent visual magnitude first drops below 20 under reasonable sky-brightness conditions, that is, with sufficient separation in the sky from the Moon and the Sun, taking into account elevation above the horizon as well as the fraction of the lunar surface that's illuminated. Column (R) lists the area of the three-sigma uncertainty ellipsoid projected in the plane of sky for the radar+optical orbit. Column (O) lists the optical-only orbit uncertainties at the time of recovery for the seven cases in which the optical-only solution predicted a recovery date within 1 month of the radar+optical prediction. The ratio O/R for those cases have a mean of 2642, providing some indication of how much larger the three-sigma search region would be with just optical data. For the six other cases, the optical-only orbit would not allow for recovery of the asteroid at all, at the time predicted; the year of most likely recovery indicated by such optical orbit solutions is in parentheses.

an orbit estimate is based on a least-squares fit to measurements of an asteroid's position over a small portion of its orbit, knowledge of the future trajectory generally is limited by statistical uncertainties that increase with the length of time from the interval spanned by astrometric measurements. Trajectory uncertainties are greatest and grow most rapidly during close planetary encounters, as the steeper gravity field gradient differentially affects the volume of space centered on the nominal orbit solution within which the asteroid is statistically located. Eventually the uncertainty region grows so large, typically within the orbit plane and along the direction of motion, that the prediction becomes meaningless.

Current ground-based optical astrometric measurements typically have angular uncertainties of between 0.2 and 1.0 arcsec (a standard deviation of 0.5 to 0.8 arcsec is common), corresponding to tens or hundreds or thousands of kilometers of uncertainty for any given measurement, depending on the asteroid's distance. Radar can provide astrometry referenced to the asteroid's center of mass, with uncertainties as small as $\sim$10 m in range and $\sim$1 mm s^{-1} in range rate. Since those measurements are orthogonal to plane-of-sky angular measurements and have relatively fine fractional precision, they offer substantial leverage on an orbit solution and normally extend NEO trajectory predictability intervals far beyond what is possible with optical data alone.

Let us define the window of predictability as the interval over which an object's Earth close approaches can be reliably known at the three-sigma level of confidence. Table 3.4 lists optical-only and radar+optical predictability windows for all radar-detected PHAs. For objects observed only during their discovery apparition, radar has enlarged the total window of predictability (past and future) by an average factor of eight, from 145 years for solutions based only on optical data to 1196 years when radar was included in the orbit solution. On average, radar has added 367 more years to the window of accurate future predictions.

When radar astrometry is excluded from the 29 single-apparition PHA radar+optical orbit solutions, 41% cannot have their next close approach predicted within the adopted confidence level using only the single apparition of optical data. This is the same percentage seen in the total population of PHAs. Radar astrometry obtained in these cases adds an average of 500 years of statistical confidence to their Earth encounter predictions, preventing them from being lost. For 2000 RD53 and 1999 FN53, the extension is through the end of this millennium.

We see that a discovery–apparition orbit solution containing radar astrometry can be compared favorably to a multiple-apparition, optical-only solution. As an example, 1998 ML14 is listed in both single and multiple apparition categories to show the effect of including the first six optical observations from the November 2002 recovery, which lengthened the data arc from 7 months to 5 years and lengthened the optical-only total knowledge window from 364 to 1721 years. By comparison,

Table 3.4 *Earth close-approach prediction intervals for radar-detected PHAs*[a]

Object		Astrometry				Earth close-approach prediction intervals						
						Optical-only		Radar+optical				
		Optical	Doppler	Delay	Days	Span	Years	Span	Years	R-O	Re-Oe	R/O
Single-apparition objects												
2000	CE59	163	2	3	210	1609–2601	992	1547–2703	1156	164	102	1.2
2002	SY50	522	2	5	72	1896–2051	155	1862–2071	209	54	20	1.3
1999	RQ36	210	1	3	208	1895–2060	165	1848–2080	232	67	20	1.4
1998	KY26	211	2	2	11	1959–2024	65	1959–2099	140	75	75	2.2
2000	QW7	850	1	0	121	1902–2087	185	1755–2185	430	245	98	2.3
2000	EW70	286	6	3	16	1971–2069	98	1929–2209	280	182	140	2.9
2000	DP107	395	1	9	250	1847–2286	439	1066–2392	1326	887	106	3.0
2000	YF29	156	2	1	207	1932–2083	151	1642–2136	494	343	53	3.3
1998	ML14	243	6	6	214	1874–2238	364	1100–2283	1183	819	45	3.3
2002	NY40	1441	5	2	35	1997–2049	52	1849–2081	232	180	32	3.5
2001	JV1	129	2	1	134	1874–2168	294	1266–2382	1116	822	214	3.8
2002	BG25	107	1	1	198	1667–2363	696	5BC–3167	3173	3172	804	4.6
2001	GQ2	323	2	1	15	1997–2084	87	1626–2100	474	387	16	5.5
2002	AY1	34	1	2	7	1848–2167	319	428–3034	2606	1842	867	8.2
2001	CP36	126	2	2	8	1972–2004	32	1628–2280	652	620	276	20.4
2000	ED14	57	1	0	16	1926–2000	74	29BC–3134	3164	3090	1134	41.8
2002	VE68	196	4	0	15	1994–2010	16	448–2653	2205	2189	643	137.8
1998	BY7	109	2	0	30	1998–1998	1	1995–1998	3	2	0	(3)
1990	OS	26	2	0	13	1990–1990	1	1966–2212	246	245	222	(246)
2002	FD6	277	2	4	15	2002–2002	1	1862–2161	299	298	159	(299)

2000	EH26	47	4	2	140	2000–2000	1	1806–2106	300	299	106	(300)
1996	JG	265	3	3	20	1996–1996	1	1851–2180	329	328	184	(329)
2000	UG11	395	1	2	19	2000–2000	1	1812–2142	330	329	142	(330)
2000	LF3	67	6	1	14	2000–2000	1	1583–2046	463	462	46	(463)
2002	BM26	218	2	2	87	2002–2002	1	1757–2312	555	554	310	(555)
2002	AV	210	3	2	39	2002–2002	1	1626–2702	1076	1075	700	(1076)
2000	RD53	322	5	4	102	2000–2000	1	1756–3023	1267	1267	1023	(1267)
2002	FC	191	3	1	137	2002–2002	1	73BC–2415	2489	2488	413	(2489)
1999	FN53	98	3	1	81	1999–1999	1	3570BC–4686	8257	8256	2687	(8256)
Mean (29)							145		1196	+1060	+367	

		Astrometry				Earth close-approach prediction intervals: Optical-only		Earth close-approach prediction intervals: Radar+optical				
Object		Optical	Doppler	Delay	Years	Span	Years	Span	Years	R-O	Re-Oe	R/O
Multiple-apparition objects												
4769	Castalia	122	7	7	13	1101–2837	1736	1043–2516	1474	–262	–321	0.8
1620	Geographos	1548	4	3	51	944–3188	2244	915–2900	1985	–259	–288	0.9
35396	(1997 XF11)	428	0	5	13	1627–2155	528	1627–2102	475	–53	–53	0.9
5604	(1992 FE)	162	0	3	17	1418–2184	766	1488–2156	668	–98	–28	0.9
6489	Golevka	686	30	26	9	1518–2706	1188	1621–2706	1085	–103	0	0.9
5189	(1990 UQ)	37	1	0	12	87BC–2660	2748	70BC–2660	2731	–17	0	1.0
49114	(1998 ST27)	287	1	3	3	1713–3775	2062	1690–3680	1990	–72	–95	1.0
25143	(1998 SF36)	628	6	10	3	1852–2170	318	1852–2170	318	0	0	1.0
4660	Nereus	371	2	11	21	1827–2166	339	1827–2166	339	0	0	1.0
7482	(1994 PC1)	268	2	0	28	1842–2361	519	1842–2361	519	0	0	1.0
	2000 EE104	319	3	0	3	1638–2351	713	1638–2351	713	0	0	1.0
2201	Oljato	187	4	0	70	1666–2392	726	1666–2392	726	0	0	1.0
	2002 HK12	516	1	0	17	1504–2299	795	1504–2299	795	0	0	1.0
4486	Mithra	233	9	8	16	1472–2255	783	1472–2281	809	26	26	1.0

Object		Astrometry				Earth close-approach prediction intervals						
						Optical-only		Radar+optical				
		Optical	Doppler	Delay	Years	Span	Years	Span	Years	R-O	Re-Oe	R/O
33342	(1998 WT24)	736	1	6	3	1751–2675	924	1751–2675	924	0	0	1.0
	1991 AQ	84	3	5	10	1786–2731	945	1786–2731	945	0	0	1.0
13651	(1997 BR)	439	1	0	20	1693–2768	1075	1693–2768	1075	0	0	1.0
4183	Cuno	495	0	1	16	>1403–2481	1078	>1403–2481	1078	0	0	1.0
4034	(1986 PA)	180	1	0	16	1424–2682	1258	1424–2682	1258	0	0	1.0
23187	(2000 PN9)	295	2	1	12	>993–2325	1332	>993–2325	1332	0	0	1.0
6037	(1988 EG)	266	4	4	13	1412–2771	1359	1377–2771	1394	35	0	1.0
2101	Adonis	54	5	0	66	1244–2609	1365	1209–2609	1400	35	0	1.0
38071	(1999 GU3)	355	6	5	13	1196–2645	1449	1196–2645	1449	0	0	1.0
52761	(1998 ML14)	249	6	6	4	562–2283	1721	562–2283	1721	0	0	1.0
10115	(1992 SK)	217	2	8	46	932–2683	1751	932–2683	1751	0	0	1.0
9856	(1991 EE)	103	1	3	10	781–2567	1780	781–2567	1780	0	0	1.0
	1999 KW4	1624	0	2	3	1145–2929	1784	1127–2929	1802	18	0	1.0
7335	(1989 JA)	137	5	0	12	1362–3219	1857	1362–3219	1857	0	0	1.0
29075	(1950 DA)	223	5	8	51	>588–2880	2292	>588–2880	2292	0	0	1.0
22753	(1998 WT)	209	1	3	47	116–2562	2446	116–2565	2449	3	3	1.0
26663	(2000 XK47)	149	2	2	27	>71BC–2397	2469	>71BC–2397	2469	0	0	1.0
1566	Icarus	624	11	0	53	1206–3803	2597	1206–3803	2597	0	0	1.0
14827	Hypnos	159	11	0	14	249–2959	2710	249–2959	2710	0	0	1.0
3908	Nyx	605	1	6	17	77BC–2708	2786	77BC-2708	2786	0	0	1.0
53319	(1999 JM8)	408	5	3	13	811–3988	3177	811–3988	3177	0	0	1.0
7822	(1991 CS)	212	4	0	11	305BC–2840	3146	305BC–2884	3191	45	44	1.0
7341	(1991 VK)	398	1	1	11	501–3797	3296	398–3797	3399	103	0	1.0
52387	(1993 OM7)	222	1	2	10	198BC–3192	3391	198BC–3207	3406	15	15	1.0
1999	FN53	133	3	1	1	3826BC–6789	10616	3826BC–6789	10616	0	0	1.0
1862	Apollo	283	8	4	71	1848–2351	503	1788–2362	574	71	11	1.1

Multiple-apparition objects												
8014	(1990 MF)	60	10	6	8	1568–2313	745	1568–2371	803	58	58	1.1
4179	Toutatis	1105	27	19	68	1221–2069	848	1117–2069	952	104	0	1.1
4953	(1990 MU)	95	2	0	27	>1519–3123	1604	>1519–3271	1752	148	148	1.1
3757	(1982 XB)	85	2	0	20	1184–2673	1489	1005–2673	1668	179	0	1.1
1981	Midas	96	1	0	26	1237–3122	1885	1011–3122	2111	226	0	1.1
Mean (45)							1803		1808	+4	–11	

[a] For each asteroid we give the time-span over which a numerically integrated orbit solution (along with its variational partial derivatives) based only on optical data can predict Earth close approaches when compared to an independent solution that also includes radar astrometry. Prediction intervals are bounded *either* by the first Earth approach ≤ 0.1 AU for which the three-sigma linearized uncertainty in the time of closest approach exceeds ± 10 days *or* by the first Earth approach for which the three-sigma approach distance uncertainty at the nominal encounter time exceeds 0.1 AU, whichever occurs first. Objects with a '>' symbol did not have any Earth approaches closer than 0.1 AU between the given year and 1000 BC, the earliest date checked. Our uncertainties are based on a mapping of the measurement covariance matrix in which the higher-order non-linear terms in the integrated variational partials are neglected. Thus, in a few cases, non-linearities due to a particularly close approach may not be immediately detected. This table includes radar-detected asteroids (Ostro 2004b) for which radar astrometry has been reported (Giorgini 2004) and which are designated PHAs by JPL or the MPC, as well as three interesting cases that are not designated PHAs (1998 KY26, 2001 CP36, and 26663 (2000 XK47)). The first four columns give the numbers of optical, Doppler, and delay measurements, and the span of time they cover. Optical-only (O) and radar+optical (R) reliable prediction date intervals are given (the actual date range as well as the number of years spanned). R-O is the difference between the radar+optical and optical-only intervals. Re-Oe is the difference in the final year of the interval; it indicates how many additional years into the future radar can predict close approaches accurately. R/O is the ratio of the total span of years for the two solutions. If the optical-only interval is unity, we place R/O in parentheses. Integrations were performed using the DE406/408 planetary ephemeris and include relativistic perturbations due to the Sun, planets, and Moon as well as asteroids Ceres, Pallas, and Vesta. Whereas this table indicates the relative effect of radar astrometry, the limits of predictability for objects having multiple planetary encounters over centuries will normally be affected by additional factors such as radiation pressure, Yarkovsky acceleration, planetary mass uncertainties, and asteroid perturbations. These factors are not included here, since the precise models are unknown and key parameters are unmeasured.

during the discovery apparition, radar astrometry combined with optical data provided an interval of 1183 years. It required the recovery of 1998 ML14 before an optical-only solution yielded a prediction interval comparable to the discovery apparition combined with radar. Similarly, for 1999 FN53, discovery apparition radar indicated an 8257-year window not possible with optical data alone until the object was recovered about half an orbit period later.

For multiple-apparition objects, radar does not significantly extend the interval, which often is terminated centuries from the present era by one or more close planetary approaches whose detailed geometry simply cannot be discerned by any present-day data type. Nevertheless, radar improves the accuracy of multi-apparition orbits. A prime example is 1950 DA: the same upper-limit of AD 2880 exists whether or not radar is included in the multiple-apparition solution. However, including radar revealed a non-negligible impact potential in 2880 not apparent in optical solutions. This was because radar astrometry eliminated a bias in the optical data and reduced the 2880 uncertainty region by about 20% as compared to the optical only solution, resulting in the potential hazard detection (see Section 4.2).

In seven of the 45 multi-apparition cases, radar astrometry actually reduced the interval of prediction, while 17 cases were slightly extended. These disparate effects arise because the different nominal orbits for the optical and optical+radar solutions have slightly different planetary encounter circumstances, so their uncertainty regions increase in different ways. Thus the net effect of radar for these multi-apparition cases is to correct the length of the optically predicted interval, suggesting that if any optical-only orbit were to reveal a potentially hazardous close approach, it would be highly desirable to get radar astrometry to check the prediction.

4 Radar and collision probability prediction

For newly discovered NEOs, a collision probability is now routinely estimated (Milani *et al*. 2002) for close Earth approaches. This probability is combined with the asteroid's estimated diameter and the time until the approach to rate the relative degree of hazard using the Palermo Technical Scale (Chesley *et al*. 2002). The Jet Propulsion Laboratory's Sentry program maintains a "risk page" (Chesley 2004) which lists objects found to have a potential for impact within the next 100 years. However, for newly discovered objects, the limited number of initial astrometric observations typically does not permit accurate trajectory prediction. When an object's optical astrometric arc is only days or weeks long, the orbit is so uncertain that a potentially hazardous close approach cannot be distinguished from a harmless one or even a non-existent one. The object is placed on the Sentry page, then

Table 3.5 *Simulated impacting orbit*

ORBIT (heliocentric J2000.0 ecliptic elements):
Impacts Earth surface: 2028-Mar-30 15:51:38.5000 (CT)
Impact relative speed: 17.26 km/s
EPOCH = 1994-Mar-05 00:00:00.0000 = 2449416.5 JD (CT)
EC = 0.50990174495185
QR = 0.93177704136264 AU
IN = 15.587556441422 deg
OM = 10.5543473199928 deg
W = 215.77334777809 deg
TP = 2449468.8313169 JD
H = 19.0
G = 0.15

typically removed later, when additional optical astrometry is obtained and the span of observations is extended. However, almost as a rule, objects on the Sentry page have not been observed with radar.

4.1 A simulated impact scenario

If an asteroid is on collision course with Earth, this fact will be recognized much sooner with radar data than without it. To examine the possible progression of optical-only and radar+optical impact probability estimates prior to a collision, we constructed a simulation as follows.

First, from the initial set of statistically possible trajectories for a recently discovered asteroid, we selected an orbit that has a 2028 approach to within two Earth radii, a 1994 approach when it could have been discovered, and two post-discovery periods of visibility. That orbit was adjusted so as to change the 2028 close approach into an impact. We adopted an absolute visual magnitude of $H = 19$, which corresponds to an object with a diameter between 420 and 940 m and having a discovery-apparition peak brightness of magnitude 14. Thirteen years after discovery, the asteroid brightens to magnitude 19, so recovery would be possible. Subsequent additional observing opportunities exist, but are less favorable since the object does not again get brighter than 20th magnitude until 9 weeks before impact. Radar observations would be possible during the discovery apparition, but then not again until 2 weeks prior to impact. Table 3.5 gives the impacting orbit and Table 3.6 lists observing opportunities.

We then simulated optical astrometry using the impacting reference trajectory and a Gaussian residual noise model in which the residual mean and standard

Table 3.6 *Observing opportunities for the simulation*

Years since discovery		Date/time	Visual brightness (magnitude)	Radar SNR	Comments
0	1994	Mar 10	16.7	–	Optical discovery
		Mar 20	15.1	532	Arecibo start
		Mar 27	14.0	17791	Last day in Arecibo window
		Mar 28	14.3	1064	Goldstone start
		Mar 30	15.2	455	Goldstone stop
		Apr 30	19.5	–	Last optical data (no impact detection)
		Oct 14	22.0	–	Last optical data (if impact detection)
13	2007	Apr 19	20.0	–	Optical recovery
		Jul 17	19.0	–	Peak brightness
		Oct 15	22.0	–	Last optical data (impact detection)
20	2014	Dec 21	21.6	–	
21	2015	Feb 21	20.0	–	Peak brightness
		Oct 14	22.0	–	
34	2028	Jan 22	20.0	–	Optical recovery
		Mar 16	16.0	15	Goldstone detection possible
		Mar 30	9.5		
		12:49:56	6.0		Dark-sky naked eye visibility
		14:01:13	5.0		
		14:45:55	4.0		
		15:12:39	3.0		
		15:29:47	2.0		
		15:40:14	1.0		
		15:46:32	0.0		
		15:50:16	–1.0		
		15:51:38	–		Surface impact

deviation for each reporting site's astrometry was based on the actual observing results for 1994 AW7. We simulated radar data for Arecibo and Goldstone using the predicted SNRs to determine observing windows and potential measurement accuracy, adjusting the astrometry to emulate the residual statistics for previous radar campaigns.

Table 3.7 shows the impact probability that would be predicted for each of several cases with different amounts of discovery-apparition radar astrometry. A typical optical campaign at discovery (case B) does not show an unusual impact risk after 50 days of observations. However, if just two radar measurements are made 10 days after discovery (case C), the likelihood of a very close approach immediately becomes evident, along with a non-negligible impact probability. Comparison of

Table 3.7 *Simulation cases and results*[a]

Cases

Discovery apparition only

Description	Data span 1994	Data span 1994	Optical	Delay	Doppler	n-RMS
(A) Optical data only	Mar 10 – Mar 21		57	0	0	0.65
(B) Optical data only	Mar 10 – Apr 30		158	0	0	0.74
(C) Optical and initial radar	Mar 10 – Mar 21		57	1	1	0.65
(D) Optical and initial radar	Mar 10 – Apr 30		158	1	1	0.73
(E) Optical and all radar	Mar 10 – Apr 01		127	11	7	0.70
(F) Optical and all radar	Mar 10 – Apr 30		158	11	7	0.73
(G) Optical and all radar	Mar 10 – Oct 16		229	11	7	0.75

Discovery apparition plus recovery apparition 13 years later

Description	Data span 1994	Data span 2007	Optical	Delay	Doppler	n-RMS
(H) 2 appar optical only	Mar 10 – Oct 15		313	0	0	0.65
(I) 2 appar optical and radar	Mar 10 – Oct 15		313	11	7	0.66

Table 3.7 (*cont.*)

Results

Nominal date (Discovery + 34 years)	± (min)	NomDist (AU)	MinDist (AU)	MaxDist (AU)	N-sigs	Volume (km^3)	Projected area (km^2)	Impact, linear	Probability, non-linear
(A) May 23.57393	± 1.0E6	0.237 217	0.203 725	2.771 532	15 902	1.3E+17	6.0E+13	0.00 000	0.000 02
(B) Apr 10.07787	± 86217	0.081 599	0.010 467	1.364 941	266 000	1.8E+10	1.1E+09	0.000 00	0.000 27
(C) Mar 30.40767	± 671	0.002 550	0.000 000	0.007 037	1.6 707	9.6E+08	6.0E+07	0.006 94	0.006 79
(D) Mar 30.73868	± 172	0.000 620	0.000 001	0.001 759	1.5 278	1.6E+07	2.0E+06	0.029 19	0.027 63
(E) Mar 30.61238	± 107	0.000 554	0.000 001	0.001 267	2.1 537	1.2E+06	1.6E+06	0.011 30	0.011 13
(F) Mar 30.65632	± 87	0.000 104	0.000 001	0.000 679	0.3 228	6.2E+05	9.1E+05	0.191 10	0.194 30
(G) Mar 30.64146	± 60	0.000 261	0.000 001	0.000 659	1.6 603	3.2E+05	6.1E+05	0.042 31	0.037 81
(H) Mar 30.66428	± 0.22	0.000 001	0.000 001	0.000 001	0.0 000	26301	1750	1.000 00	1.000 00
(I) Mar 30.66426	± 0.20	0.000 001	0.000 001	0.000 001	0.0 000	894	1433	1.000 00	1.000 00

[a] For each case in our simulation, the top part of the table indicates the number of optical and radar astrometric measurements, their date span, and the normalized root mean squares residual. In the "Results" section at the bottom, the first columns give the encounter time and its three-sigma uncertainty. NomDist is the solution's nominal (highest probability), numerically integrated Earth approach distance on the given date. MinDist and MaxDist are the minimum and maximum (three-sigma) approach distances from the linearized covariance mapping. N-sigs is the number of standard deviations required for the mapped covariance ellipsoid to intersect the surface of the Earth. The next columns give the volume of the three-sigma uncertainty region and the area it projects into a plane perpendicular to the impactor's velocity vector at encounter. The last columns give the impact probabilities computed by the linearized mapping method and by the non-linear method used by Sentry, JPL's automated hazard monitoring system.

cases A and C reveals that after the first two radar measurements, the volume of the uncertainty region is nine orders of magnitude smaller with the radar+optical orbit than with the optical-only orbit.

At the conclusion of case B's 50-day observing window, a 0.027% impact probability is indicated by the optical-only solution. This is noteworthy, but not unusual for single-apparition objects – there currently are four objects on the Sentry Risk Page with a comparable impact probability. However, with the radar astrometry (case F), a 19% impact probability is indicated at the same point in time. Radar reduces the volume of the uncertainty region at the encounter by five orders of magnitude compared to the optical-only case B. A 19% impact probability would attract additional resources and would extend the window of optical observability several months, down to at least magnitude 22 (case G). Due to marginally greater bias and noise in the simulated data as the target fades from view, the additional optical astrometry moves the solution's nominal close approach slightly further away from the Earth, decreasing the impact probability estimate.

If instead there is no radar data at the discovery apparition, recovery would probably still occur during the optically favorable apparition 13 years after discovery. If so, two such apparitions of optical data conclusively identify the impact event whether or not radar data is available (cases H and I), although the radar data reduces the volume of the uncertainty region by a factor of 29 compared to a solution based only on two apparitions of optical data. However, if the recovery does not occur, the next good opportunity to recover the object and clarify the impact risk, or perhaps to first become aware of it, would be 2 months prior to impact. Radar data during the discovery apparition guarantees the recovery by clearly indicating a high impact risk immediately, providing 34 years of warning instead of 21 years (or possibly only a few weeks).

4.2 Negative predictions, positive predictions, and warning time

To a great extent, the dominance of PHA trajectory uncertainties is a temporary one, an artifact of the current discovery phase. Predictions are made for single-apparition objects having a few days or weeks of measurements. The uncertainty region in such cases can encompass a large portion of the inner solar system, thereby generating small but finite impact probabilities that change rapidly as the data arc lengthens, or if high-precision radar delay and Doppler measurements can be made. Impact probabilities in such cases are effectively a statement that the motion of the asteroid is so poorly known that the Earth cannot avoid passing through the asteroid's large uncertainty region – hence the apparent impact "risk." As optical measurements are made, the region shrinks. The resulting change in impact probability, up or down, is effectively a statement about where the asteroid won't be – a "negative

prediction" – rather than a "positive prediction" of where it will be. This is due to the modest positional precision of optical measurements.

In contrast, radar measurements naturally provide strong constraints on the motion and hence "positive predictions" about where an asteroid will be decades and often centuries into the future. *Thus radar measurements substantially open the time-window of positive predictability*. However, within a couple of decades, asteroids being found now (but unobserved by radar) will themselves have multiple optical apparitions and similarly be predictable in a positive way over centuries, as radar cases are now. In this way, orbit uncertainties for present-day radar cases illustrate what the situation will be by mid-century for most of the asteroids known today, and presumably for almost all PHAs as large as 1 kilometer.

Unless a significant impact is predicted to occur in the next few decades, mitigation will primarily be an issue for multi-apparition asteroids with decades of observations behind them (since most objects will typically have that much optical astrometry) or for radar-detected objects, with the impact predictions at least centuries in the future. Examination of the next 1000 years will be 30 times as likely to find an actual impactor than examination of the next few decades. This suggests that high-energy mitigation methods may be rendered obsolete before they could be implemented, not by technology, but by the changing nature of orbit predictability as the primary discovery phase ends and observations accumulate. Low-energy methods such as radiation pressure or Yarkovsky modification can potentially be implemented at lower cost, on timescales compatible with the actual hazard.

4.3 1950 DA

At this writing, there is only one known NEO with a potentially significant possibility of collision. For 29075 (1950 DA), integrations of the radar-refined orbit by Giorgini *et al*. (2002) revealed that in 2880 there could be a hazardous approach not indicated in the half-century arc of pre-radar optical data. The current nominal orbit represents a risk as large as 50% greater than that of the average background hazard due to all other asteroids from now through 2880, as defined by the Palermo Technical Scale (PTS value +0.17). 1950 DA is the only known asteroid whose danger could be above the background level. During the observations, a radar time-delay measurement corrected the optical ephemeris's prediction by 7.9 km, changing an optical-only prediction of a 2880 close approach to a nominal distance of 20 lunar distances into a radar-refined prediction of a nominal distance of 0.9 lunar distances.

The uncertainty in the closeness of 1950 DA's 2880 approach and hence in the probability of a collision (which could be as low as zero or as high as 1/300) is due

Table 3.8 *Sources of uncertainty in 1950 DA's position during the 2880 close approach*[a]

Phenomenon	Relative maximum along-track effect
Galilean satellites	1.0 (3100 km, 4 min)
Galactic tide	2.7
Numerical integration error	3.2
Solar mass loss	4.3
Poynting–Robertson drag	7.7
Solar oblateness	13.6
61 most perturbing "other" asteroids	484
Planetary mass uncertainty	496
Solar radiation pressure	3613
Yarkovsky effect	22903

[a] These factors are normally neglected in asteroid trajectory predictions spanning less than a century. From Giorgini *et al*. (2002).

to a combination of the factors in Table 3.8. The dominant factor is the Yarkovsky acceleration, which is due to the anisotropic reradiation of absorbed sunlight as thermal energy and depends on the object's mass, size, shape, spin state, and global distribution of optical and thermal properties. Thus, unlike previous cases, predicting a potential 1950 DA impact with the Earth depends mostly on the asteroid's physical characteristics, not initial trajectory measurement. The accelerations are all small, but add up over time and are amplified by 15 close encounters with the Earth or Mars prior to 2880.

The 1950 DA example underscores the fundamental inseparability of the physical properties of NEAs and long-term prediction of their trajectories. The urgency of physically characterizing a threatening object naturally would increase as estimates of the collision probability rise and mitigation is transformed from a hypothetical possibility to an engineering requirement. If we take the hazard seriously, physical characterization of these objects deserves high priority.

5 Physical characterization

5.1 Images and physical models

With adequate orientational coverage, delay-Doppler images can be used to construct three-dimensional models (e.g., Hudson *et al*. 2000), to define the rotation state, and to constrain the internal density distribution. Even a single echo spectrum jointly constrains the target's size, rotation period, and sub-radar latitude. A series of Doppler-only echo spectra as a function of rotation phase can constrain the location

of the center of mass with respect to a pole-on projection of the asteroid's convex envelope (e.g., Benner *et al*. 1999a). For objects in a non-principal-axis spin state, the hypothesis of uniform internal density can be tested directly (Hudson and Ostro 1995). Given a radar-derived model and the associated constraints on an object's internal density distribution, one can use a shape model to estimate the object's gravity field and hence its dynamical environment, as well as the distribution of gravitational slopes on the surface, which can constrain regolith depth and interior configuration.

For most NEAs, radar is the only Earth-based technique that can make images with useful spatial resolution. Therefore, although a sufficiently long, multi-apparition optical astrometric time base might provide about as much advance warning of a possibly dangerous close approach as a radar+optical data set, the only way to compensate for a lack of radar images is with a space mission.

5.2 Extreme diversity

As reviewed by Ostro *et al*. (2002), NEA radar has revealed both stony and metallic objects, principal-axis and complex rotators, very smooth and extraordinarily rough surfaces, objects that must be monolithic and objects that almost certainly are not, spheroids and highly elongated shapes, objects with complex topography and convex objects virtually devoid of topography, contact binaries, and binary systems. Figure 3.2 illustrates some of the diversity of NEAs. Obviously it is useless to talk about the physical characteristics of a "typical" PHA.

5.3 Surface roughness and bulk density

Porous, low-strength materials are very effective at absorbing energy (Asphaug *et al*. 1998). The apparently considerable macroporosity of many asteroids (Britt *et al*. 2002) has led Holsapple (2002) to claim that impact or explosive deflection methods may be ineffective, even for a non-porous asteroid if it has a low-porosity regolith only a few centimeters deep: "That leaves the low force, long time methods. However, even in those cases the problems of anchoring devices to the surface may make them very difficult."

The severity of surface roughness would be of concern to any reconnaissance mission designed to land or gather samples. The wavelengths used for NEAs at Arecibo (13 cm) and Goldstone (3.5 cm), along with the observer's control of the transmitted and received polarizations, make radar experiments sensitive to the surface's bulk density and to its roughness at centimeter to meter (cm-to-m) scales (e.g., Magri *et al*. 2001). An estimate of the surface bulk density offers a safe lower bound on the subsurface bulk density, and hence a lower bound on the

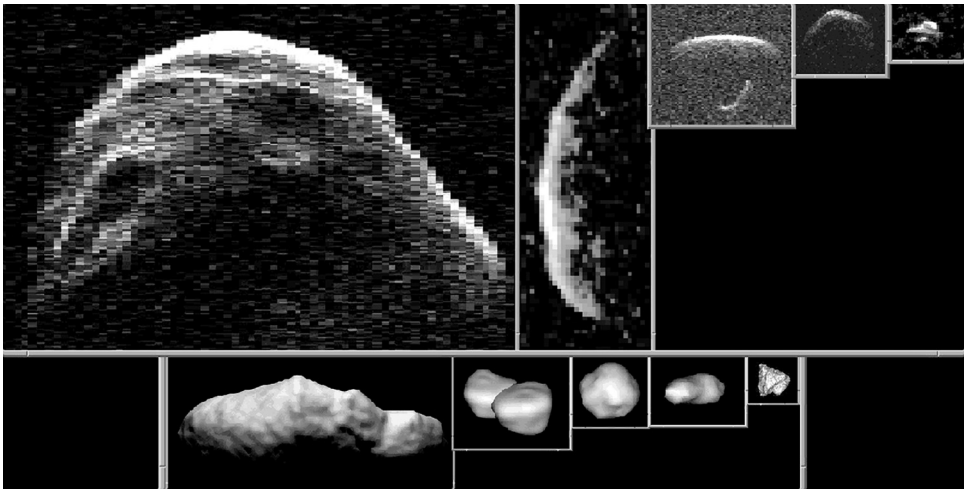

Figure 3.2 Radar delay-Doppler images and shape models. The top collage shows radar images of (left to right) 1999 JM8 (Benner *et al*. 2002a), Geographos (Ostro *et al*. 1996), the binary 1999 KW4 (Ostro *et al*. 2002), 1950 DA (Giorgini *et al*. 2002), and Golevka (Hudson *et al*. 2000). The bottom collage shows renderings of shape models of (left to right) Toutatis (Hudson *et al.* 2003), Castalia (Hudson and Ostro 1994), Nyx (Benner *et al.* 2002b), Bacchus (Benner *et al*. 1999b), and Golevka (Hudson *et al*. 2000). The relative scale of the images and models is approximately correct; Nyx is about 1 km in diameter.

asteroid's mass. Bulk density is a function of regolith porosity and grain density, so if an asteroid can confidently be associated with a meteorite type, then the average porosity of the surface can be estimated. Values of porosity estimated by Magri *et al*. (2001) for nine NEAs range from 0.28 to 0.78, with a mean and standard deviation of 0.53 ± 0.15. The current results suggest that most NEAs are covered by at least several centimeters of porous regolith, and therefore the above warning by Holsapple may be valid for virtually any object likely to threaten collision with Earth.

The fact that NEAs' circular polarization ratios (SC/OC) range from near zero to near unity (Fig. 3.3) means that the cm-to-m structure on these objects ranges from negligible to much more complex than any seen by the spacecraft that have landed on Eros (whose SC/OC is about 0.3, near the NEA average), the Moon, Venus, or Mars. 2101 Adonis and 1992 QN (Benner *et al*. 1997) and 2000 EE104 (Howell *et al*. 2001) are the extreme examples, with SC/OC near unity.

Ostro *et al*. (2002) claim that an asteroid's SC/OC can be taken as a crude estimate of the fraction of the surface area covered by roughly wavelength-sized rocks. To what extent might the surface rock coverage be representative of the structural configuration inside the object? NEA surfaces apparently can have rock coverages

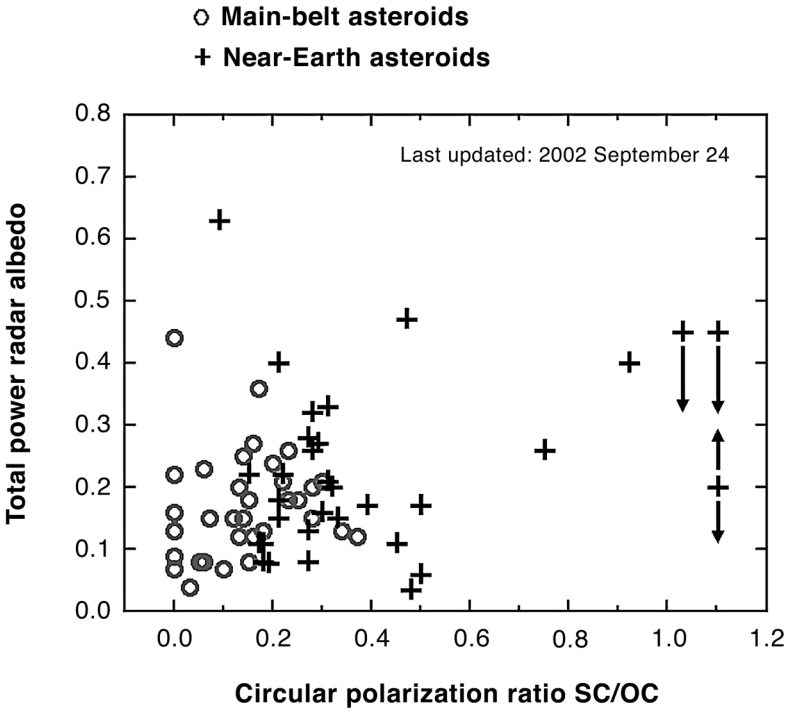

Figure 3.3 Radar properties of NEAs and mainbelt asteroids. The two crosses with single arrows give upper bounds on the albedo; the cross with two arrows indicates an unknown albedo.

anywhere from negligible to total, and NEA interiors apparently can lie anywhere in the Richardson *et al*. (2002) relative-tensile-strength-vs.-porosity parameter space. Is there any relation between the two? If so, then an object's radar properties may indicate possibilities for its interior and hence for mitigation options. If not, then those properties still constrain options for spacecraft surface operations.

5.4 Binary NEAs: mass and density

The most basic physical properties of an asteroid are its mass, its size and shape, its spin state, and whether it is one object or two. The current Arecibo and Goldstone systems are able to identify binary NEAs unambiguously and at this writing have imaged 13 (Margot *et al*. 2002, and references therein; Nolan *et al*. 2002; references listed in Ostro 2004b), all of which are designated PHAs. Current detection statistics, including evidence from optical lightcurves (Pravec 2004) suggest that between 10% and 20% of PHAs are binary systems.

Analysis of echoes from these binaries is yielding our first measurements of PHA densities. Delay-Doppler images of 2000 DP107 (Margot *et al*. 2002) reveal a 800-m primary and a 300-m secondary. The orbital period of 1.767 d and semi-major axis of 2620 $\pm$ 160 m yield a bulk density of 1.7 $\pm$ 1.1 g cm^{-3} for the primary. DP107 and the five other radar binaries have spheroidal primaries spinning near the breakup-point for strengthless bodies. Whether binaries' components were mutually captured following a highly dispersive impact into a much larger body (Richardson *et al*. 2002, and references therein) or formed by tidal disruption of an object passing too close to an inner planet (Margot *et al*. 2002), it seems likely that the primaries are unconsolidated, gravitationally bound aggregates, so Holsapple's warning applies to them.

5.5 Radar investigations, mission design, and spacecraft navigation

Whether a PHA is single or binary, mitigation will involve spacecraft operations close to the object. Maneuvering near a small object is a non-trivial challenge, because of the weakness and complexity of the gravitational environment (Scheeres *et al*. 2000). Maneuvering close to either component of a binary system would be especially harrowing.

The instability of close orbits looms as such a serious unknown that unless we have detailed information about the object's shape and spin state, it would be virtually impossible to design a mission capable of autonomous navigation close to the object. Control of a spacecraft orbiting close to an asteroid requires knowledge of the asteroid's location, spin state, gravity field, size, shape and mass, as well as knowledge of any satellite bodies that could pose a risk to the spacecraft. Radar can provide information on all these parameters. Knowledge of the target's spin state as well as its shape (and hence nominal gravity harmonics under the assumption of uniform density) (Miller *et al*. 1999) would permit design of stable orbits immune to escape or unintended surface impact. (Upon its arrival at Eros, the NEAR Shoemaker spacecraft required almost 2 months to refine its estimate of the gravity field enough to ensure reliable close-approach operations.)

If it turns out to be necessary to have a sequence of missions beginning with physical reconnaissance and ending with a deflection, then a radar-derived physical model would speed up this process, reduce its cost, decrease complexity in the design and construction of the spacecraft, and improve the odds of successful mitigation. A reduced need for contingency fuel could be significant enough to allow a smaller launch vehicle for the mission. For example, the result might save $100 million via a switch from a Titan III launch vehicle to a Titan IIS, or $200 million for a switch from a Titan IV to a Titan III. The ability of prior radar

reconnaissance to reduce mission cost, complexity and risk was embraced by the Department of Defense in their proposed Clementine II multiple-flyby mission (Hope *et al*. 1997), all of whose candidate targets either had already been observed with radar (Toutatis, Golevka) or were radar observable prior to encounter (1987 OA, 1989 UR).

Ironically, although PHAs include the lowest-ΔV rendezvous targets in the solar system, Japan's Hayabusa (MUSES-C) sample-return mission to 25143 Itokawa (1998 SF36) is the world's first rendezvous mission to a PHA. Results of radar imaging of that asteroid (Ostro *et al*. 2001) are being used by the Japanese Institute of Space and Astronautical Science in planning for the late 2005 rendezvous, and radar observations during the asteroid's mid-2004 close approach will be used for navigational assistance and to refine the model derived from the 2001 images. Radar-derived shape models of small NEAs have made it possible to explore the evolution and stability of close orbits (e.g., Scheeres *et al*. 1996, 1998), and this experience is currently being applied to Hayabusa.

Radar refinement of physical properties and radar refinement of orbits are very tightly coupled: shape modeling necessarily involves refinement of the delay-Doppler trajectory of the center of mass through the observing ephemerides. With very precise radar astrometry, a spacecraft lacking onboard optical navigation could be guided into orbit around, or collision course with, an asteroid. For example, consider how Goldstone observations shrunk the positional error ellipsoid of Geographos, an object already heavily observed by optical telescopes, just prior to a planned Clementine flyby of that target on August 31, 1994 (Ostro 1996). Before Goldstone ranging observations carried out during August 28–29, the overall dimension of the positional error ellipsoid was $\sim$11 km. The radar astrometry collapsed the ellipsoid's size along the line of sight to several hundred meters, so its projection toward Clementine on its inbound leg would have been 11 $\times$ 2 km. Goldstone–VLA radar aperture synthesis angular astrometry (see discussions by de Pater *et al*. 1994, and Hudson *et al*. 2000), could have shrunk the error ellipsoid's longest dimension to about 1 km, about half of Geographos' shortest overall dimension. For less well-observed objects, the gains could be substantially more, as with 1862 Apollo's 3750 km radar range correction.

5.6 Modeling the efficiency of explosive deflection

Mitigation scenarios include the use of explosives to deflect the projectile (Ahrens and Harris 1992). However, as demonstrated by Asphaug *et al*. (1998), the outcome

of explosive energy transfer to an asteroid or comet (via a bomb or a hypervelocity impact) is extremely sensitive to the pre-existing configuration of fractures and voids, and also to impact velocity. Just as porosity damps shock propagation, sheltering distant regions from impact effects while enhancing energy deposition at the impact point, parts of multi-component asteroids are preserved, because shock waves cannot bridge inter-lobe discontinuities. A radar-derived shape model would allow more realistic investigation (Asphaug *et al*. 1998) of the potential effectiveness of nuclear explosions in deflecting or destroying a hazardous asteroid.

5.7 Comets

The risk of a civilization-ending impact during this century is about the same as the risk of a civilization-ending impact by a long-period comet (LPC) during this millennium. At present, the maximum possible warning time for an LPC impact probably is between a few months and a few years. Comet trajectory prediction is hampered by optical obscuration of the nucleus and by uncertainties due to time-varying, non-gravitational forces. Comets are likely to be very porous aggregates, so concern about the ineffectiveness of explosive deflection is underscored in the case of comets.

Radar reconnaissance of an incoming comet would be the most reliable way to estimate the size of the nucleus (Harmon *et al*. 1999), could reveal the prevalence of centimeter-and-larger particles in the coma (Harmon *et al*. 1989, 1997), and would be valuable for determining the likelihood of a collision.

6 Recommendations

How much effort should be made to make radar observations of NEAs? For newly discovered objects, it is desirable to guarantee recovery and to ensure accurate prediction of close approaches well into the future, and at least throughout this century. Moreover, a target's discovery apparition often provides the most favorable radar opportunity for decades and hence a unique chance for physical characterization that otherwise would require a space mission. Similarly, even for NEAs that have already been detected, any opportunity offering a significant increment in echo strength and hence imaging resolution should be exploited. Binaries and non-principal-axis rotators, for which determination of dynamical and geophysical properties requires a long, preferably multi-apparition time base, should be observed extensively during any radar opportunity.

Construction of the proposed Large Synoptic Survey Telescope (LSST) has been endorsed (Belton *et al*. 2002), in part as a means to extend the Spaceguard Survey's

90% completeness goal for kilometer-sized objects down to 300-m objects. However, both Arecibo and Goldstone are already heavily oversubscribed, with only several percent of their time available for asteroid radar. Over the coming decades, it may become increasingly clear that most of the NEO radar reconnaissance that is technically achievable with Arecibo and Goldstone is precluded by the limited accessibility of those instruments, and that a dedicated NEO radar instrument is desirable.

An ideal NEO radar system (Ostro 1997) might consist of two antennas like the 100-m NRAO Greenbank Telescope (GBT, in West Virginia), one with a megawatt transmitter and one just for receiving, separated by a few tens of kilometers, operating at a wavelength of 0.9 cm (Ka band). Each antenna's gain could be 88 dB, compared to 73.5 dB for Arecibo. A two-antenna (bistatic) configuration would eliminate the frequent transmit/receive alternation and klystron power cycling required in single-antenna observations of NEOs and would double the available integration time. The antennas would be fully steerable, so any object could be tracked at least several times longer than at Arecibo. The combination of all these factors would make this dedicated NEO radar an order of magnitude more sensitive than the upgraded Arecibo telescope. The capital cost of building this system now, as calibrated by the GBT experience, would be within 10% of $180 million, comparable to the cost of a small Discovery mission and very close to the estimated cost of the LSST.

Acknowledgment

This research was conducted at the Jet Propulsion Laboratory, California Institute of Technology, under contract with the National Aeronautics and Space Administration (NASA). S. Ostro was partially supported by the Steven and Michele Kirsch Foundation.

References

Ahrens, T. J. and Harris, A. W. 1992. Deflection and fragmentation of near-Earth asteroids. *Nature* **360**, 429–433.

Asphaug, E., Ostro, S. J., Hudson, R. S., *et al*. 1998. Disruption of kilometre-sized asteroids by energetic collisions. *Nature* **393**, 437–440.

Beatty, J. K. 2002. Arecibo radar gets 11th-hour reprieve. Sky Publishing Corp. [cited April 23, 2004]. Available online at http://skyandtelescope.com/news/archive/article_285_1.asp.

Belton, M. J., Porco, C., A'Hearn, M., *et al*. (2002). *New Frontiers in the Solar System: An Integrated Exploration Strategy Solar System Exploration Survey*. Washington, DC: National Research Council.

Benner, L. A. M., Ostro, S. J., Giorgini, J. D., *et al*. 1997. Radar detection of near-Earth asteroids 2062 Aten, 2101 Adonis, 3103 Eger, 4544 Xanthus, and 1992 QN. *Icarus* **130**, 296–312.

Benner, L. A. M., Ostro, S. J., Rosema, K. D., *et al*. 1999a. Radar observations of asteroid 7822 (1991 CS). *Icarus* **137**, 247–259.

Benner, L. A. M., Hudson, R. S., Ostro, S. J., *et al*. 1999b. Radar observations of asteroid 2063 Bacchus. *Icarus* **139**, 309–327.

Benner, L. A. M., Ostro, S. J., Nolan, M. C., *et al*. 2002a. Radar observations of asteroid 1999 JM8. *Meteor. and Planet. Sci*. **37**, 779–792.

Benner, L. A. M., Ostro, S. J., Hudson, R. S., *et al*. 2002b. Radar observations of asteroid 3908 Nyx. *Icarus* **158**, 379–388.

Britt, D. T., Yeomans, D., Housen, K., *et al*. 2002. Asteroid density, porosity, and structure. In *Asteroids III*, eds. W. F. Bottke, A. Cellino, P. Paolicchi, and R. P. Binzel, pp. 485–500. Tucson, AZ: University of Arizona Press.

Chesley, S. R. 2004. Current impact risks. California Institute of Technology, Pasadena [cited April 23, 2004]. Available online at http://neo.jpl.nasa.gov/risks.

Chesley, S. R., Chodas, P. W., Milani, A., 2002. Quantifying the risk posed by potential Earth impacts. *Icarus* **159**, 423–432.

de Pater, I., Palmer, P., Mitchell, D. L., *et al*. 1994. Radar aperture synthesis observations of asteroids. *Icarus* **111**, 489–502.

Giorgini, J. D. 2004. Small-body astrometric radar observations. California Institute of Technology, Pasadena [cited April 23, 2004]. Available online at http://ssd.jpl.nasa.gov/radar_data.html.

Giorgini, J. D., Ostro, S. J., Benner, L. A. M., *et. al.* 2002. Asteroid 1950 DA's encounter with Earth in 2880: physical limits of collision probability prediction. *Science* **296**, 132–136.

Goldstein, R. M. 1968. Radar observations of Icarus. *Science* **162**, 903–904.

Harmon, J. K., Campbell, D. B., Hine, A. A., *et al.* 1989. Radar observations of comet IRAS-Araki-Alcock 1983d. *Astroph. J*. **338**, 1071–1093.

Harmon, J. K., Ostro, S. J., Benner, L. A. M., *et al*. 1997. Comet Hyakutake (C/1996 B2): radar detection of nucleus and coma. *Science* **278**, 1921–1924.

Harmon, J. K., Campbell, D. B., Ostro, S. J., *et al*. 1999. Radar observations of comets. *Planet. Space Sci*. **47**, 1409–1422.

Holsapple, K. A. (2002). The deflection of menacing rubble pile asteroids. In *Extended Abstracts from the NASA Workshop on Scientific Requirements for Mitigation of Hazardous Comets and Asteroids*, Arlington, VA, September 3–6, 2002, eds. E. Asphaug and N. Samarasinha. pp. 49–52.

Hope, A. S., Kaufman, B., Dasenbrock, R., *et al*. 1997. A Clementine II mission to the asteroids. In *Dynamics and Astrometry of Natural and Artificial Celestial Bodies, Proceedings of IAU Colloquium 165*, eds. I. M. Wytrzyszczak, J. H. Lieske, and R. A. Feldman, pp. 183–190. Dordrecht, The Netherlands: Kluwer.

Howell, E. S., Nolan, M. C., DeRemer, L., *et al*. 2001. Arecibo radar observations of near-Earth asteroid 2000 EE104. *Bull. Am. Astron. Soc.*, **33**, 1153.

Hudson, R. S. and Ostro, S. J. 1994. Shape of asteroid 4769 Castalia (1989 PB) from inversion of radar images. *Science* **263**, 940–943.

1995. Shape and non-principal-axis spin state of asteroid 4179 Toutatis. *Science* **270**, 84–86.

Hudson, R. S., Ostro, S. J., Jurgens, R. F., *et al*. 2000. Radar observations and physical modeling of asteroid 6489 Golevka. *Icarus* **148**, 37–51.

Hudson, R. S., Ostro, S. J., and Scheeres, D. J. 2003. High-resolution model of asteroid 4179 Toutatis. *Icarus* **161**, 348–357.

Magri, C., Consolmagno, G. J., Ostro, S. J., *et al*. 2001. Radar constraints on asteroid regolith compositions using 433 Eros as ground truth. *Meteor. and Planet. Sci*. **36**, 1697–1709.

Margot, J. L., Nolan, M. C., Benner, L. A. M., *et al*. 2002. Binary asteroids in the near-Earth object population. *Science* **296**, 1445–1448.

Milani, A., Chesley, S. R., Chodas, P. W., *et al*. 2002. Asteroid close approaches: analysis and potential impact detection. In *Asteroids III*, eds. W. F. Bottke, A. Cellino, P. Paolicchi, and R. P. Binzel, pp. 55–69. Tucson, AZ: University of Arizona Press.

Miller, J. K., Antreasian., P. J., Gaskell, R. W., *et al*. 1999. Determination of Eros physical parameters for near-Earth asteroid rendezvous orbit phase navigation. *Am. Astron. Soc*. Paper no. 99-463.

Morrison, D., Harris, A. W., Sommer, G., *et al*. 2002. Dealing with the impact hazard. In *Asteroids III*, eds. W. F. Bottke, A. Cellino, P. Paolicchi, and R. P. Binzel, pp. 739–754. Tucson, AZ: University of Arizona Press.

Nolan, M. C., Howell, E. S., Ostro, S. J., *et al*. 2002. 2002 KK_8. *IAU Circ. No.* **7921**.

Ostro, S. J. 1994. The role of groundbased radar in near-Earth object hazard identification and mitigation. In *Hazards due to Comets and Asteroids*, eds. T. Gehrels, pp. 259–282. Tucson, AZ: University of Arizona Press.

1996. Radar astrometry of asteroids, comets and planetary satellites. In *Dynamics and Ephemerides of the Solar System, Proceedings of IAU Symposium 172*, eds. S. Ferraz-Mello, B. Morando, and J.-E. Arlot, pp. 365–372. Dordrecht, The Netherlands: Kluwer.

1997. Radar reconnaissance of near-Earth objects at the dawn of the next millennium. *Ann. New York Acad. Sci.* **822**, 118–139.

2004a. Echo strength predictions. California Institute of Technology, Pasadena [cited April 23, 2004]. Available online at http://echo.jpl.nasa.gov/∼ostro/snr/.

2004b. Radar-detected asteroids. California Institute of Technology, Pasadena [cited April 23, 2004]. Available online at http://echo.jpl.nasa.gov/ asteroids/index.html.

Ostro, S. J., Campbell, D. B., Chandler, J. F., *et al*. 1991. Asteroid radar astrometry. *Astron. J*. **102**, 1490–1502.

Ostro, S. J., Jurgens, R. F., Rosema, K. D., *et al.* 1996. Radar observations of asteroid 1620 Geographos. *Icarus* **121**, 44–66.

Ostro, S. J., Benner, L. A. M., Nolan, M. C., *et al*. 2001. Radar observations of asteroid 25143 (1998 SF36). *Bull. Am. Astron. Soc.* **33**, 1117.

Ostro, S. J., Hudson, R. S., Benner, L. A. M., *et al*. 2002. Asteroid radar astronomy. In *Asteroids III*, eds. W. F. Bottke, A. Cellino, P. Paolicchi, and R. P. Binzel, pp. 151–168. Tucson, AZ: University of Arizona Press.

Pettengill, G. H., Shapiro, I. I., Ash, M. E., *et al*. 1969. Radar observations of Icarus *Icarus*, **10**, 432–435.

Pravec, P. 2004. Binary near-Earth asteroids. Ondrejov Observatory [cited April 23, 2004]. Available online at http://www.asu.cas.cz/∼asteroid/binneas.htm.

Richardson, D. C., Leinhardt, Z. M., Melosh, H. J., *et al*. 2002. Gravitational aggregates: evidence and evolution. In *Asteroids III*, eds. W. F. Bottke, A. Cellino, P. Paolicchi, and R. P. Binzel, pp. 501–515. Tucson, AZ: University of Arizona Press.

Scheeres, D. J., Ostro, S. J., Hudson, R. S., *et al*. 1996. Orbits close to asteroid 4769 Castalia. *Icarus* **121**, 67–87.

1998. Dynamics of orbits close to asteroid 4179 Toutatis. *Icarus* **132**, 53–79.

Scheeres, D. J., Williams, B. G., and Miller, J. K. 2000. Evaluation of the dynamic environment of an asteroid: applications to 433 Eros. *J. Guidance, Control and Dynamics* **23**, 466–475.

Shapiro, I. I., Ash, M. E., and Smith, W. B. 1968. Icarus: further confirmation of the relativistic perihelion precession. *Phys. Rev. Lett*. **20**, 1517–1518.

Yeomans, D. K., Ostro, S. J., and Chodas, P. W. 1987. Radar astrometry of near-Earth asteroids. *Astron. J*. **94**, 189–200.

Zellner, B. 1979. Asteroid taxonomy and the distribution of the compositional types. In *Asteroids*, ed. T. Gehrels, pp. 783–806. Tucson, AZ: University of Arizona Press.